RAA 2021 Vol. **21** No. **4**, 82(9pp) doi: 10.1088/1674-4527/21/4/82

http://www.raa-journal.org *http://iopscience.iop.org/raa*

***R**esearch in*
***A**stronomy and*
***A**strophysics*

Portable adaptive optics for exoplanet imaging

Yong-Tian Zhu[1,2,3], Jiang-Pei Dou[1,2], Xi Zhang[1,2], Gang Zhao[1,2], Jing Guo[1,2] and Leopoldo Infante[4,5,6]

[1] National Astronomical Observatories / Nanjing Institute of Astronomical Optics & Technology, Chinese Academy of Sciences, Nanjing 210042, China; *jpdou@niaot.ac.cn*
[2] Key Laboratory of Astronomical Optics & Technology, Nanjing Institute of Astronomical Optics & Technology, Chinese Academy of Sciences, Nanjing 210042, China
[3] School of Astronomy and Space Sciences, University of Chinese Academy of Sciences, Beijing 100049, China
[4] Las Campanas Observatory, Observatories of the Carnegie Institution of Washington, Colina El Pino S/N Casilla 601 La Serena, Chile
[5] Institute of Astrophysics, Pontificia Universidad Católica de Chile, Av. Vic Mackenna 4860, Santiago, Chile
[6] Núcleo de Astronomía de la Facultad de Ingeniería y Ciencias, Universidad Diego Portales, Manuel Rodríguez Sur 415, Santiago, Chile

Received 2020 January 20; accepted 2020 October 19

Abstract The portable adaptive optics (PAO) device is a low-cost and compact system, designed for 4-meter class telescopes that have no adaptive optics (AO) system, because of the physical space limitation at the Nasmyth or Cassegrain focus and the historically high cost of conventional AO. The initial scientific observations of the PAO are focused on the direct imaging of exoplanets and sub-stellar companions. This paper discusses the concept of PAO and the associated high-contrast imaging performance in our recent observational runs. PAO deliver a Strehl ratio better than 60% in H band under median seeing conditions of $1''$. Combined with our dedicated image rotation and subtraction (IRS) technique and the optimized IRS (O-IRS) algorithm, the averaged contrast ratio for a $5 \leq V_{\rm mag} \leq 9$ primary star is 1.3×10^{-5} and 3.3×10^{-6} at angular distance of $0.36''$ with exposure time of 7 minutes and 2 hours, respectively. PAO has successfully revealed the known exoplanet of κ And b in our recent observation with the 3.5-meter ARC telescope at Apache Point Observatory. We have performed the associated astrometry and photometry analysis of the recovered κ And b planet, which gives a projected separation of $0.984'' \pm 0.05''$, a position angle of $51.1^\circ \pm 0.5^\circ$ and a mass of $10.15^{+2.19}_{-1.255}\,M_{\rm Jup}$. These results demonstrate that PAO can be used for direct imaging of exoplanets with medium-sized telescopes.

Key words: stars: imaging — instrumentation: adaptive optics — instrumentation: high angular resolution — methods: observational — techniques: image processing

1 INTRODUCTION

With over 3800 already known exoplanets, most of them were discovered by indirect detection approaches including transit and radial velocity. However, the direct imaging method has become increasingly important, since it can spatially separate the light of a planet from the host star. It has opened a window for the spectroscopy analysis of the atmosphere of the planet, thus eventually allowing the detection of terrestrial biology signals in future space missions. With a high-contrast imaging technique, several giant planets have been detected at relatively large orbital separations by ground-based observations (Macintosh et al. 2015). The HR 8799 system with four giant planets, for instance, has been observed and recovered mostly by current 8–10 meter class telescopes (Marois et al. 2008; 2010). The existence of giant planets at large angular separations has challenged the current planet formation model. However, the amount of exoplanets detected by direct imaging is still low compared with other indirect detection approaches. It therefore requires more high-contrast imaging instruments and associated scientific observations on as many telescopes as possible, including small-sized telescopes with 2–4 meter aperture.

Most of the exoplanets discovered through direct imaging are, in general, young and self-luminous, and have large orbital separations, which make them possible

to be imaged in infrared and resolved with small telescopes. Such observation with a small-sized telescope was demonstrated in Serabyn et al. (2010). With a 1.5-meter aperture telescope, three of the exoplanets in the HR 8799 system were also revealed by utilizing an extreme adaptive optics (ExAO) system that delivers a Strehl ratio (SR) of 0.91 at the near infrared (NIR) K band (Serabyn et al. 2010). High-contrast imaging with small telescopes would be especially important for these time-intensive surveys (Mawet et al. 2009).

We proposed and built the first portable adaptive optics (PAO) system that is optimized for exoplanet high-contrast imaging with current 2–4 meter class telescopes since 2013. By employing a small-aperture deformable mirror (DM) with the micro-electro-mechanical systems (MEMS) technique and rapid programming with LabVIEW based control software, the PAO features a compact physical size, low cost, high performance and high flexibility that make it able to work with any size telescope. Operating the PAO with a "small" telescope can provide a high SR, since a DM with a moderate number of actuators can be used and high speed AO correction is achievable.

One of the critical issues for exoplanet high-contrast imaging is the so called non-common path aberrations (NCPA). Both GPI and SPHERE follow the two-step approach, which requires a post calibration interferometer or phase-diversity algorithm to measure the differential aberration then command the DM to correct it (Hinkley et al. 2009; Fusco et al. 2006; Sauvage et al. 2007). In 2012, we presented a unique technique that employs the focal plane point spread function (PSF) information to directly command the DM to correct the NCPA, which was based on an iterative optimization algorithm (Dou et al. 2011; Ren et al. 2012a). The approach can correct the differential aberration in a single step, which locks on a wavefront with accuracy on the order of 7.4×10^{-4} of the working wavelength.

PAO has been used as a visiting instrument at European Southern Observatory's (ESO's) 3.6-meter New Technology Telescope (NTT) and the 3.5-meter Astrophysics Research Consortium (ARC) telescope at Apache Point Observatory (APO). In recent observation, PAO has successfully recovered the known exoplanet κ And b under a medium seeing condition. With optimized image rotation and subtraction (O-IRS) reduction, it has delivered contrast ratios of 1.3×10^{-5} and 3.3×10^{-6} at angular distance of $0.36''$ under exposure times of 7 minutes and 2 hours, respectively.

In this paper, we present the development and performance of PAO during recent observations. In Section 2, we review the development history of PAO. In Section 3, we describe the design and associated performance of PAO and provide the observation results, especially the analysis of the recovered planet of κ And b. Conclusions and future work will be presented in Section 4.

2 PAO HISTORY

PAO is a nighttime AO system that originated from the Portable Solar Adaptive Optics (PSAO) system. PSAO was initially proposed for diffraction-limited imaging of the Sun (Ren et al. 2009). PSAO has been fully tested with different solar telescopes at different seeing conditions, in which it could always deliver good performance (Ren et al. 2010; Ren & Dong 2012; Ren et al. 2012a; Ren & Zhu 2013).

We then developed PAO from PSAO by simply replacing the cross-correlation module for daytime wavefront sensing with the centroid-calculation module for nighttime wavefront sensing. The first PAO test observation was conducted in 2013, in which the white dwarf Sirius B in a binary system was clearly imaged, at National Solar Observatory's (NSO's) 1.6-meter McMath-Pierce (McMP) Solar Telescope (Ren et al. 2014).

PAO was then updated and firstly optimized for a 4-meter class telescope for more experimental observations since 2014. The PAO prototype system employed a DM with 97 actuators. With 9×9 wavefront sensor (WFS) sub-apertures, PAO can stably work with a correction speed at 1000 Hz. The first engineering observation was carried out at the ESO 3.6-meter NTT telescope in Chile in July, 2014. Six nights were approved by ESO and the observation program was collaborated with the Pontificia Universidad Católica de Chile, with the support of Chinese Academy of Sciences South America Center for Astronomy (CASSACA). But due to strong wind at the site, the system was only allowed to operate for 3 nights during our 6-night observation run, however it was the first time to demonstrate that our PAO is able to rapidly be connected to a 4-meter class telescope and provide effective corrections.

Figure 1 shows the 3.6-meter NTT telescope (left panel) and our PAO interfaced with the telescope's Nasmyth B (NB) port (right panel).

Figure 2 displays an example of a PSF before AO correction (panel a)), after AO correction (panel b)) and finally processed with O-IRS (panel c)). The achieved contrast is plotted in panel d). Here we use 144 frames with each frame having less than a 3 second exposure time, which gives a 7 minute integration time in total. The blue, red and green lines correspond to the direct combination, LOCI (Lafrenière et al. 2007) and O-IRS reduction respectively (Ren et al. 2012b; Dou et al. 2015). An initial contrast ratio on the order of 10^{-4} has

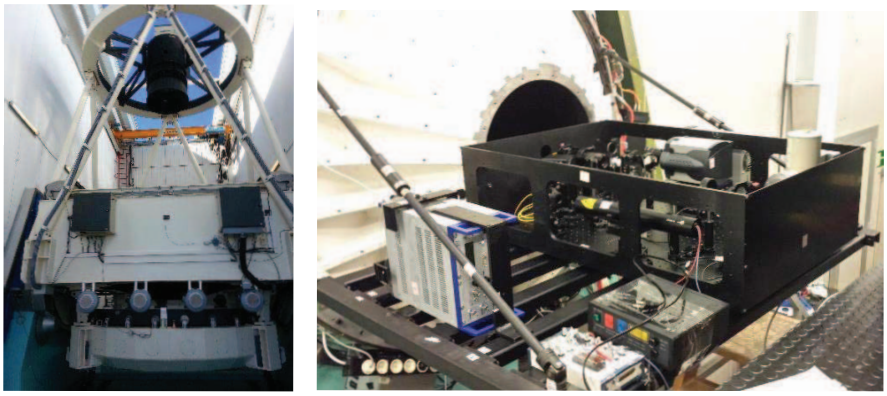

Fig. 1 The 3.6-meter NTT telescope (*left*) and PAO installed on NB (*right*).

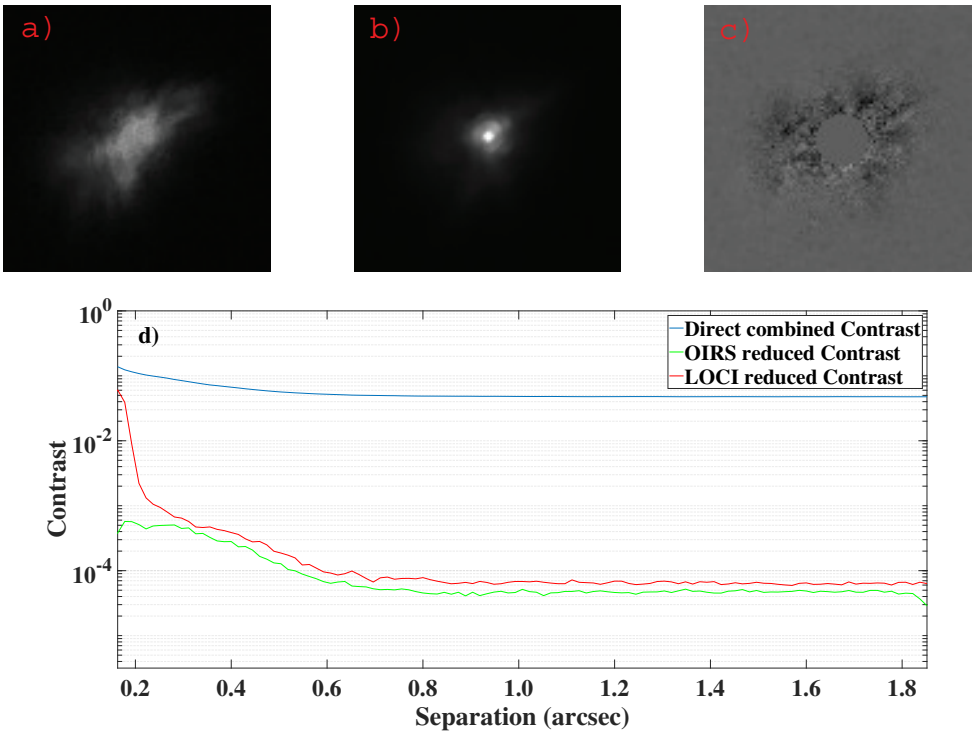

Fig. 2 An example of high-contrast reduction for H band observation of the star Fomalhaut.

been achieved at an angular separation of $0.5''$. The above engineering observation clearly demonstrates the feasibility of our PAO technique.

3 PAO DESCRIPTION

After fully demonstrating that the PAO can be utilized for scientific exoplanet imaging, we applied and purchased more observational time on the 3.5-meter ARC telescope, with the goal to further explore and improve the PAO's capabilities for exoplanet imaging.

3.1 Optical Layout and Expected Performance

To further improve the high contrast performance, PAO was finally updated and optimized for the 3.5-meter ARC telescope at APO. Figure 3 illustrates the optical layout of the PAO for the 3.5-meter ARC telescope. The light from the telescope focus TF (f/# 10.35) is collimated by the cemented doublet lens with a focal length of 150 mm, in order to match the clear aperture of the DM of 13.5 mm. The tip-tilt mirror (TTM) is positioned behind the collimator for overall tip-tilt correction. The light propagates to the DM, which corrects possible wavefront errors. A dichroic beam-splitter (BS) is located behind the DM. Visible light is reflected by the BS to the WFS

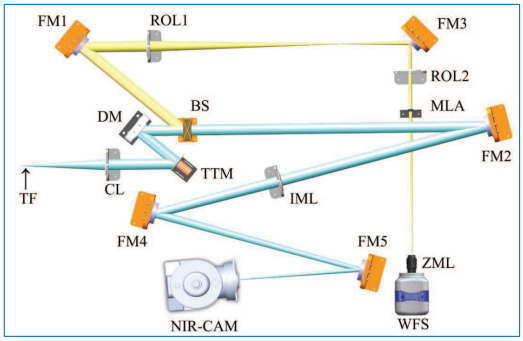

Fig. 3 Optics layout of PAO optimized for exoplanet scientific observation.

for wavefront sensing, while infrared light continuously propagates to a science NIR camera, where a high-contrast image is formed on the focal plane IM at f/50 by the Imaging Lens. The whole PAO system was constructed in a $0.9 \times 0.78 \times 0.3\,\mathrm{m}^3$ self-contained enclosed box that will be installed on the ARC Nasmyth A (NA) Port.

Employing a high speed 97-element DM and an EMCCD as the WFS camera, PAO could achieve a maximum speed of 1300 Hz for open-loop correction. Table 1 lists the PAO specifications and estimated performances. The PAO used the DM-97 with a correction speed increased to 2000 Hz, with 10 μm wavefront stroke. The TTM is mounted on the PI's S-330.4SL piezo tip/tilt platform. The optical deflection angle in the two orthogonal axes is 10 mrad and the tilt/tilt platform can achieve a resonance frequency of about 1600 Hz (loaded). The WFS has 9×9 sub-apertures (excluding those in the four corners), and each sub-aperture will be sampled by 4×4 pixels on the WFS camera. The WFS camera is an EMCCD purchased from Photometrics. It has 512×512 pixels (16×16 μm pixel size), with less than $1\,e^-$ readout noise in EM gain mode, and can deliver a frame rate of 1820 Hz for our PAO with a region of 64×64 pixels. The science camera is an NIR camera from Xenics.

The error budget of our AO with the Shack-Hartmann (SH) WFS can be calculated as the residual variance

$$\sigma^2 = \sigma^2_{\mathrm{fit}} + \sigma^2_r + \sigma^2_{\mathrm{ph}} + \sigma^2_{\mathrm{bw}}, \qquad (1)$$

where σ^2_{fit} is the fitting error that represents the wavefront variance due to the limited DM actuator number compared to the telescope aperture, σ^2_r is WFS read noise error, σ^2_{ph} is the photon noise error and σ^2_{bw} is the lag error due to finite AO bandwidth. The fitting error is determined by the actuator number which is 97. The read noise is determined by the WFS camera readout noise which is $(0.15\,e^-)$. The photon noise is determined by the NGS magnitude and sub-aperture size. The lag error is determined by the AO correction speed which is 1300 Hz and average wind speed which is $20\,\mathrm{m\ s}^{-1}$.

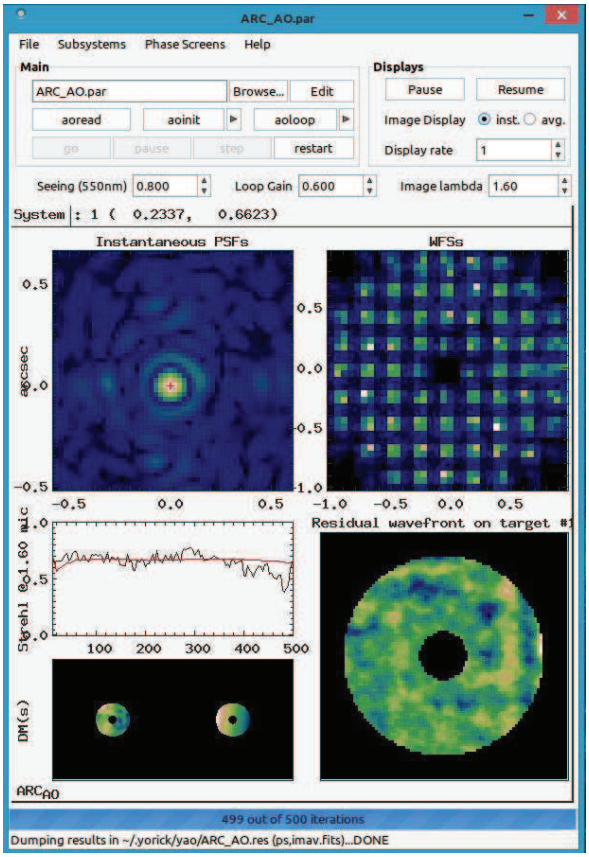

Fig. 4 YAO interface for PAO performance simulation.

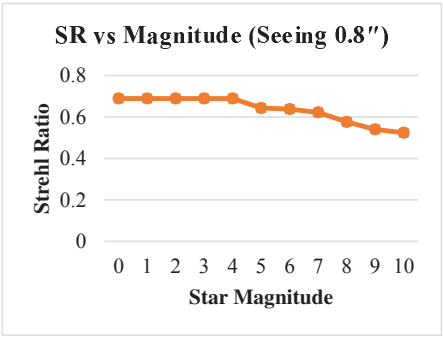

Fig. 5 Expected SR correction performance of PAO for different magnitude stars.

For small residual variance, the SR can be calculated by employing the analytical equation $S = \exp(-\sigma^2)$. Precisely evaluating the above errors depends on many factors including seeing parameter r_0, NGS brightness, telescope aperture size and its central obstruction, sub-aperture number of SH WFS, as well as the telescope and SH WFS/DM geometric configurations and other properties, which involve a complicated analytical process. Here we calculate the SR employing the end-to-end software YAO simulation software package (*http://frigaut.github.io/yao/*), with all above error

Table 1 AO Hardware Specifications and Performance for Bright NGSs in Good Seeing $r_0 = 13$ cm

Hardware	Specifications
DM	97 actuators in 10×10 configuration, $+/-$ 5-μm wavefront stroke, 13.5 mm clear aperture, 2000 Hz frame rate
TTM	PI S-330.4SL, 5 mrad stroke range, 1600 Hz frame rate
WFS	9×9 Shack-Hartmann sub-apertures, 4×4 pixels / sub-aperture
WFS camera	Photometrics Evolve-512 Delta EMCCD, 1820 Hz at 64×64 pixels
AO correction speed	1300 Hz
Computer	$4 \times$ 12-core Intel Xeon® E5-4657L v2 2.4 GHz (48 cores total)
Field of view	$30'' \times 30''$
SR at m_v = 5	0.64 at H
SR at m_v = 10	0.52 at H

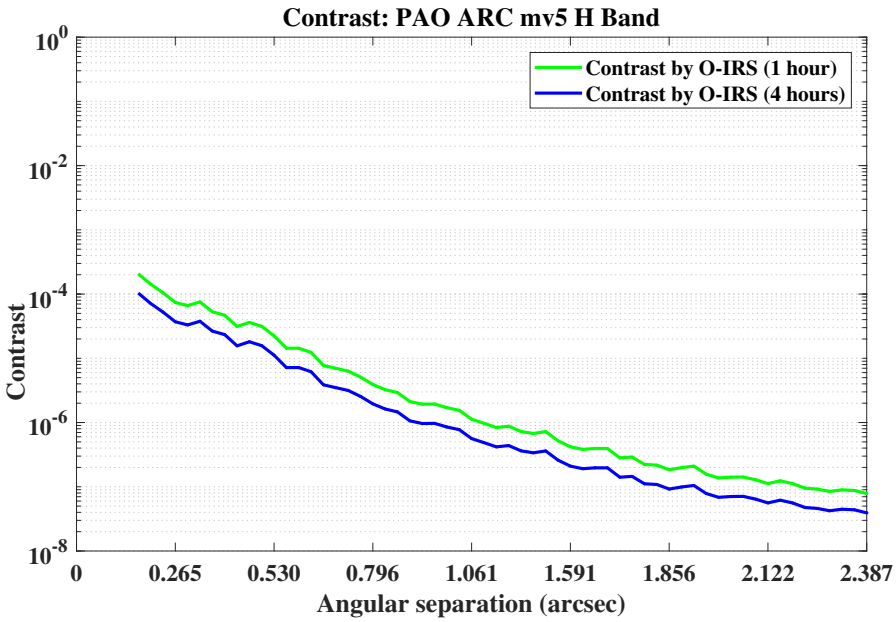

Fig. 6 Expected contrast performance of PAO for $m_v = 5$ star at H band.

sources and configurations inputted (fitting error, read noise, photon noise, bandwidth, telescope and WFS/DM geometric configurations, etc.), which yields more realistic results. Figure 4 displays the interface of the YAO software for simulation of the PAO correction of bright stars. Since the non-common-path error will be corrected by our SPGD algorithm, it is not included in the above calculation/simulation. The AO performance is a function of the seeing condition as well as the guide star brightness. At good seeing, $r_0 = 13$ cm at 500 nm and SR is 0.64 at the H (1.60 μm) band, for a natural guide star with $m_v = 5$, as shown in Table 1 and Figure 5. The AO should deliver better performance in excellent seeing conditions.

The simulation software YAO can calculate the PAO instantaneous PSF. The AO corrected PSFs are variable with a period of speckle lifetime t_0, which is determined as $t_0 = 0.6D/v$ (Macintosh et al. 2005), where D is telescope aperture diameter and v is the atmospheric wind speed. For an AO system with the NCPA corrected, the contrast can be improved by increasing the exposure time, with improvement factor of $\sqrt{T/t_0}$, where T is the exposure time. Figure 6 depicts the expected achievable contrast for the H band exoplanet imaging with $m_v = 5$ NGS with exposure times of 1 hour and 4 hours. These are achieved by utilizing our unique O-IRS reduced instantaneous PSFs, each with an exposure of speckle lifetime (Dou et al. 2015). The simulation results demonstrate that the PAO can deliver contrasts of 10^{-6} and $10^{-6.5}$ at an angular separation of $1''$, for exposures of 1 hour and 4 hours respectively.

3.2 PAO Performance at 3.5-meter ARC Telescope

3.2.1 Observation of the binary stars HR 6212 A and B

Six observation runs were conducted at the 3.5-meter ARC telescope at APO during 2015 to 2018. Figure 7 displays

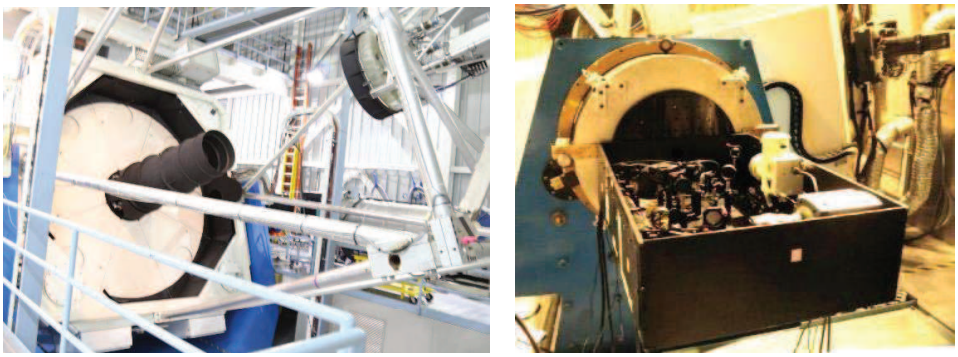

Fig. 7 The 3.5-meter ARC telescope (*left*) and the PAO installed on NA2 port (*right*).

Fig. 8 HR 6212 A/B images before (*left*) and after (*right*) PAO correction at 3.5-meter ARC telescope.

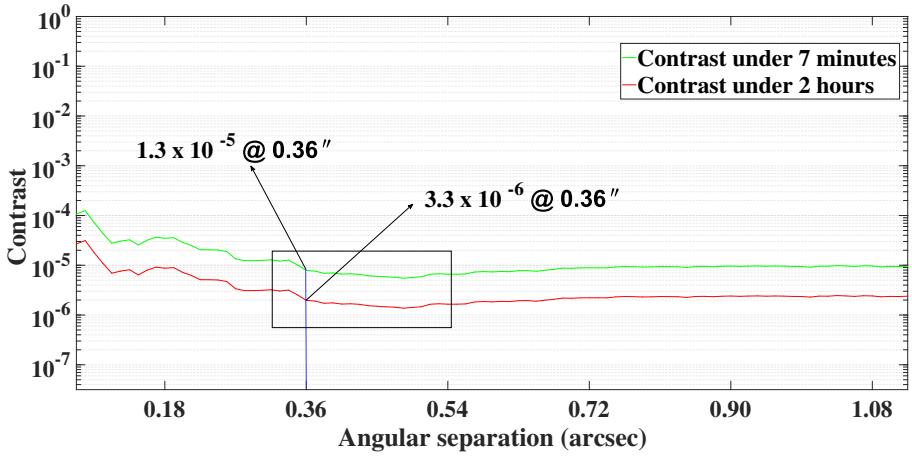

Fig. 9 Contrast achieved with PAO at the 3.5-meter ARC telescope.

the 3.5-meter ARC telescope (left panel) and our PAO interfaced with the telescope's NA2 port (right panel).

The first two runs were carried out in 2015. A couple of targets were used to test PAO potential performance for high-contrast imaging. Figure 8 features the AO on and off correction of the binary stars HR 6212 A and B, in which the companion star B is clearly visible after PAO correction. Figure 9 showcases the associated contrast achieved with the APO 3.5-meter telescope with an exposure of 7 minutes after O-IRS data reduction. A contrast of 1.3×10^{-5} was achieved at an inner working angle of $0.36''$, corresponding to $4\lambda/D$, four times the coronagraph diffraction beam, which implies that the contrast of 3.3×10^{-6} should be achievable with a longer exposure time of 2 hours. The ExAO systems in routine operation such as GPI and SPHERE on 8-meter telescopes exhibit better performance than the current PAO, which can deliver better imaging contrasts of 10^{-6} from an angular distance of $0.3''$, considering that the ExAOs rely on denser sub-apertures to sample the telescope pupil. However,

Fig. 10 The observed κ And image after PAO correction with seeing of $1''$.

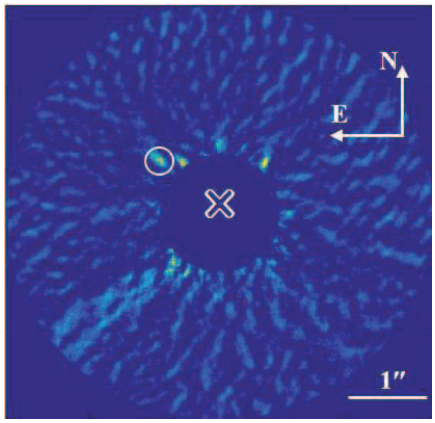

Fig. 11 The reduced image of planet κ And b; the star center is marked with a cross.

the PAO still shows its capability at imaging exoplanets and brown dwarfs on medium-sized telescopes. The data reduction was conducted by applying our O-IRS algorithm (Dou et al. 2015). This result clearly indicates that our PAO is a mature technique and is ready to be utilized for scientific exoplanet imaging.

3.2.2 Observation of the known exoplanet κ And b

We firstly conducted the high-contrast imaging observation of κ And b in 2014 in H band with the 3.5-meter ARC at APO to test PAO's capability for direct imaging of giant exoplanets around young stars. The planet κ And b was firstly imaged in 2012 by utilizing the Subaru/HiCIAO during the SEEDS survey (Carson et al. 2013) and then characterized by the subsequent Keck and Large Binocular Telescope Observatory (LBTI) high-contrast observations in 2012 and 2013 (Bonnefoy et al. 2014). These observations were carried out in J, H, Ks and Lp infrared bands. Since our current NIR camera is cut-off at 1.55 μm, in this observation run, we only consider H band data for the purpose of demonstration.

The observation was carried out with the NIR camera using the 640×512 pixel array in angular differential imaging (ADI) mode without any field rotation compensation. All frames of the host star κ And were acquired with 2 second exposure time without saturation for the following photometric measurement to derive the flux ratios, in order to compare this observation result with the previous ones. The data were saved in a cube with 50 frames in each cube and 23 cubes in total. The integration time of all cubes was 2300 s with a small field rotation of 8.83 degrees. Figure 10 displays one single frame image of κ And after PAO correction.

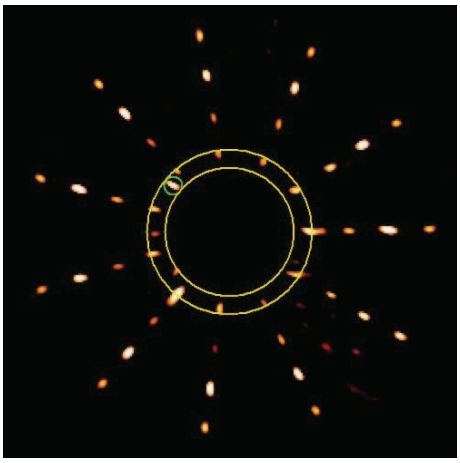

Fig. 12 The reduced image of κ And with artificial planets added: the location of planet b is marked in the *green circle*, while the *yellow annulus* signifies the second innermost artificial planets with the same angular separation as planet b.

3.3 Data Reduction

The raw images were processed based on our recently developed data reduction pipeline for high contrast imaging (Dou et al. 2015). We firstly carried out the basic reduction including bad pixels and cosmic rays, dark current, flat field and background calibrations; then these images were registered and speckle suppression was conducted based on O-IRS and principal component analysis (PCA), respectively (Ren et al. 2012b; Dou et al. 2015; Amara & Quanz 2012; Otten et al. 2017). The pipeline is written in both IDL and Python, well-known and frequently used languages in astronomical environments.

Meanwhile, we performed the astrometry analysis of planet b, in which we took into account the positional uncertainties of the centroid errors of the companion,

Table 2 Astrometry Analysis of Planet κ And b

Date	H band (1.63 μm)		Ks (2.65 μm)		H band (1.55 μm)	
	Proj. sep. ($''$)	Proj. ang. ($''$)	Proj. sep. ($''$)	Proj. ang. ($''$)	Proj. sep. ($''$)	Proj. ang. ($''$)
2012 January 1	1.070 ± 0.010	55.7 ± 0.6				
2012 July 8	1.058 ± 0.007	56.0 ± 0.4				
2012 October 30			1.029 ± 0.005	55.3 ± 0.3		
2012 November 3						
2017 June 10					0.984 ± 0.05	51.1 ± 0.5
Reference	[1]		[2]		[3]	

References: [1] Carson et al. 2013; [2] Bonnefoy et al. 2014; [3] this work.

Table 3 Photometry Analysis of Planet κ And b

Planets	J band (1.25μm)	H band (1.63μm)	H band (1.55μm)	Ks (2.65μm)	L' (3.8μm)	NB (4.05μm)	M (4.7μm)
κ And b	15.86 ± 0.21	14.95 ± 0.13	15.145 ± 0.195	14.32 ± 0.09	13.12 ± 0.1	13.0 ± 0.2	13.3 ± 0.3
	16.3 ± 0.3	15.2 ± 0.2		14.6 ± 0.4	13.12 ± 0.09		
Reference	[1], [2]	[1], [2]	[3]	[1], [2]	[1], [2]	[1]	[1]

References: [1] Bonnefoy et al. 2014; [2] Carson et al. 2013; [3] this work.

and systematic errors in the distortion solution and the north/west alignment. For the orientation alignment, we recorded two cubes of images when first moving the telescope toward north (distance of $2.7''$) then to the east (distance of $2.9''$). The image rotation angle was calculated by using the center of the median of all images in the two cubes, which gives a rotation angle of $4.5° \pm 0.5°$ to align the north orientation with the y axis of the image. The pixel scale of the PAO image is found to be $0.024''$ pixel^{-1}. Finally, the reduced image of κ And b processed by the PCA-based algorithm was de-rotated by $4.5°$ and is displayed in Figure 11. Table 2 lists the astrometry analysis results based on previous observation in 2012–2013 and in this observation.

We then performed the photometry analysis of the reduced planets. A series of artificial planets were added in the same data of κ And after basic reduction with a certain contrast, following a similar procedure that was used in previous work (Lafrenière et al. 2007; Dou et al. 2015). In each frame of the data set, planets are inserted at eleven different azimuth angles. In order to cover the region where planet b is located, here several artificial planets along one radius were added, in which the second innermost one has an angular separation of $0.984''$, the same as planet b. The final frame has a field rotation of 8.83 degrees, which is also the same as the data set. Then the speckle suppression based on O-IRS and PCA is carried out on these images in the data set. Figure 12 features the reduced image with artificial planets, when adjusting the intensity of the artificial planet to be the same as that of planet b. It finally gives a contrast of $4.691 \pm 0.85 \times 10^{-5}$, which corresponds to a magnitude of 15.145 ± 0.195 at 1.55 μm. In Figure 12, an annulus between $0.895''$ and $1.072''$ was added to cover the location of planet κ And b. The signal to noise ratio (S/N) of the planet was calculated, which is 7.75σ.

A summary of the available photometry is presented in Table 3. Here we apply the same physical parameters of the primary star of κ And b as the work in Carson et al. (2013), in which the estimated age is 30^{+20}_{-10} Myr, and the parallax is 19.2 ± 0.7 (Perryman et al. 1997). The H band (1.55 μm) magnitude is 15.145 ± 0.195 which gives a mass of $10.15^{+2.19}_{-1.255}\, M_{\rm Jup}$ and a temperature of $1227^{+4}_{-4.5}$ K by employing the BT-DUSTY evolutionary models (Chabrier & Baraffe 2000; Spiegel & Burrows 2012).

4 CONCLUSIONS

In this paper, we have briefly reviewed the development history of the PAO technique. We then updated PAO to be a visiting instrument that is optimized for the direct imaging of exoplanets and sub-stellar companions. The unique feature of PAO is its compact physical size and high performance which allows it to be used for direct imaging of exoplanets with current 3–4 meter class telescopes. In the most recent observation at the 3.5-meter ARC telescope at APO, we successfully recovered the known exoplanet of κ And b reduced by utilizing our unique O-IRS and PCA algorithms. The observation contrast reached 10^{-5} at an angular distance from $0.36''$ to $1''$. Finally, we performed the associated astrometry and photometry analysis of the recovered κ And b planet, which is consistent with previous work. It has been fully demonstrated that our portable high-contrast imaging system can be used for direct imaging observation of exoplanets with medium-sized telescopes.

Acknowledgements This work was supported by the National Natural Science Foundation of China (Grant Nos. 11827804 and U2031210).

References

Amara, A., & Quanz, S. P. 2012, MNRAS, 427, 948
Bonnefoy, M., Currie, T., Marleau, G. D., et al. 2014, A&A, 562, A111
Carson, J., Thalmann, C., Janson, M., et al. 2013, ApJL, 763, L32
Chabrier, G., & Baraffe, I. 2000, ARA&A, 38, 337
Dou, J.-P., Ren, D.-Q., & Zhu, Y.-T. 2011, RAA (Research in Astronomy and Astrophysics), 11, 198
Dou, J., Ren, D., Zhao, G., et al. 2015, ApJ, 802, 12
Fusco, T., Petit, C., Rousset, G., et al. 2006, in Proc. SPIE, 6272, 62720K
Hinkley, S., Oppenheimer, B. R., Soummer, R., et al. 2009, ApJ, 701, 804
Lafrenière, D., Marois, C., Doyon, R., et al. É. 2007, ApJ, 660, 770
Macintosh, B., Poyneer, L., Sivaramakrishnan, A., & Marois, C. 2005, in Proc. SPIE, 5903, 59030J
Macintosh, B., Graham, J., Barman, T., et al. 2015, Science, 350, 64
Marois, C., Macintosh, B., Barman, T., et al. 2008, Science, 322, 1348
Marois, C., Zuckerman, B., Konopacky, Q. M., et al. 2010, Nature, 468, 1080
Mawet, D., Serabyn, E., Stapelfeldt, K., & Crepp, J. 2009, ApJL, 702, L47
Otten, G. P. P. L., Snik, F., Kenworthy, M. A., et al. 2017, ApJ, 834, 175
Perryman, M. A. C., Lindegren, L., Kovalevsky, J., et al. 1997, A&A, 323, L49
Ren, D., & Dong, B. 2012, Opt. Eng., 51, 101705
Ren, D., Dong, B., Zhu, Y., & Christian, D. J. 2012a, PASP, 124, 247
Ren, D., Dou, J., Zhang, X., & Zhu, Y. 2012b, ApJ, 753, 99
Ren, D., Penn, M., Plymate, C., et al. 2010, in Proc. SPIE, 7736, 77363P
Ren, D., Penn, M., Wang, H., Chapman, G., & Plymate, C. 2009, in Proc. SPIE, 7438, 74380P
Ren, D., & Zhu, Y. 2013, in Adaptive Optics Progress, ed. R. K. Tyson (Rijeka: IntechOpen)
Ren, D., Li, R., Zhang, X., et al. 2014, in Proc. SPIE, 9148, 91482W
Sauvage, J.-F., Fusco, T., Rousset, G., & Petit, C. 2007, J. Opt. Soc. Am. A, 24, 2334
Serabyn, E., Mawet, D., & Burruss, R. 2010, Nature, 464, 1018
Spiegel, D. S., & Burrows, A. 2012, ApJ, 745, 174